Important Notice to Authors

> **No further publication processing will occur until we receive your response to this proof.**

Attached is a PDF proof of your forthcoming article in PRA. Your article has 7 pages and the Accession Code is **AS11658**.

Please note that as part of the production process, APS converts all articles, regardless of their original source, into standardized XML that in turn is used to create the PDF and online versions of the article as well as to populate third-party systems such as Portico, Crossref, and Web of Science. We share our authors' high expectations for the fidelity of the conversion into XML and for the accuracy and appearance of the final, formatted PDF. This process works exceptionally well for the vast majority of articles; however, please check carefully all key elements of your PDF proof, particularly any equations or tables.

Figures submitted electronically as separate files containing color appear in color in the online journal. However, all figures will appear as grayscale images in the print journal unless the color figure charges have been paid in advance, in accordance with our policy for color in print (https://journals.aps.org/authors/color-figures-print).

Specific Questions and Comments to Address for This Paper

1. Please check size of figure 4. Is enlargment required?
2. Journal style would prefer a page range to a chapter number. Are these authors the authors of the entire book or is this an edited/contributed book? If the latter, please give name/s of editor/s.
3. Journal style would prefer a page or page range to a section.

FQ: This funding provider could not be uniquely identified during our search of the FundRef registry (or no Contract or Grant number was detected). Please check information and amend if incomplete or incorrect.

Q: This reference could not be uniquely identified due to incomplete information or improper format. Please check all information and amend if applicable.

Open Funder Registry: Information about an article's funding sources is now submitted to Crossref to help you comply with current or future funding agency mandates. Crossref's Open Funder Registry (https://www.crossref.org/services/funder-registry/) is the definitive registry of funding agencies. Please ensure that your acknowledgments include all sources of funding for your article following any requirements of your funding sources. Where possible, please include grant and award ids. Please carefully check the following funder information we have already extracted from your article and ensure its accuracy and completeness:

Coordenação de Aperfeiçoamento de Pessoal de Nível Superior (BR)

Other Items to Check

- Please note that the original manuscript has been converted to XML prior to the creation of the PDF proof, as described above. Please carefully check all key elements of the paper, particularly the equations and tabular data.
- Title: Please check; be mindful that the title may have been changed during the peer-review process.
- Author list: Please make sure all authors are presented, in the appropriate order, and that all names are spelled correctly.
- Please make sure you have inserted a byline footnote containing the email address for the corresponding author, if desired. Please note that this is not inserted automatically by this journal.
- Affiliations: Please check to be sure the institution names are spelled correctly and attributed to the appropriate author(s).
- Receipt date: Please confirm accuracy.
- Acknowledgments: Please be sure to appropriately acknowledge all funding sources.
- Hyphenation: Please note hyphens may have been inserted in word pairs that function as adjectives when they occur before a noun, as in "x-ray diffraction," "4-mm-long gas cell," and "R-matrix theory." However, hyphens are deleted from word pairs when they are not used as adjectives before nouns, as in "emission by x rays," "was 4 mm in length," and "the R matrix is tested."

  Note also that Physical Review follows U.S. English guidelines in that hyphens are not used after prefixes or before suffixes: superresolution, quasiequilibrium, nanoprecipitates, resonancelike, clockwise.
- Please check that your figures are accurate and sized properly. Make sure all labeling is sufficiently legible. Figure quality in this proof is representative of the quality to be used in the online journal. To achieve manageable file size for online delivery, some compression and downsampling of figures may have occurred. Fine details may have become somewhat fuzzy, especially in color figures. The print journal uses files of higher resolution and therefore details may be sharper in print. Figures to be published in color online will appear in color on these proofs if viewed on a color monitor or printed on a color printer.
- Please check to ensure that reference titles are given as appropriate.
- Overall, please proofread the entire *formatted* article very carefully. The redlined PDF should be used as a guide to see changes that were made during copyediting. However, note that some changes to math and/or layout may not be indicated.

Ways to Respond

- *Web:* If you accessed this proof online, follow the instructions on the web page to submit corrections.
- *Email:* Send corrections to praproofs@aptaracorp.com
    - Subject: **AS11658** proof corrections
- *Fax:* Return this proof with corrections to +1.703.791.1217. Write **Attention:** PRA Project Manager and the Article ID, **AS11658**, on the proof copy unless it is already printed on your proof printout.

Quadrature histograms in maximum-likelihood quantum state tomography

J. L. E. Silva,[1] S. Glancy,[2] and H. M. Vasconcelos[1,2,*]

[1]*Departamento de Engenharia de Teleinformática, Universidade Federal do Ceará, Fortaleza, Ceará, 60440, Brazil*

[2]*Applied and Computational Mathematics Division, National Institute of Standards and Technology, Boulder, Colorado 80305, USA*

Quantum state tomography aims to determine the quantum state of a system from measured data and is an essential tool for quantum information science. When dealing with continuous variable quantum states of light, tomography is often done by measuring the field amplitudes at different optical phases using homodyne detection. The quadrature-phase homodyne measurement outputs a continuous variable, so to reduce the computational cost of tomography, researchers often discretize the measurements. We show that this can be done without significantly degrading the fidelity between the estimated state and the true state. This paper studies different strategies for determining the histogram bin widths. We show that computation time can be significantly reduced with little loss in the fidelity of the estimated state when the measurement operators corresponding to each histogram bin are integrated over the bin width.

I. INTRODUCTION

Quantum information science and engineering have advanced to the point where rudimentary quantum computers are available in the laboratory and commercially [1–4]. However, further advancing quantum technologies requires improvements in the fidelities of basic operations. Consequently, more precise and efficient reconstruction and diagnostic tools for estimation of quantum states [5–12], processes [13–20], and measurements [21–24] are essential. Quantum tomographic techniques for optical quantum states of light have become standard tools because quantum light sources are essential for implementations of continuous-variable quantum computation and communication [25–29]. These sources are also extensively exploited in quantum cryptography [30–34], quantum metrology [35,36], state teleportation [37–39], dense coding [40,41], and cloning [42,43].

In the quantum state tomography studied here, one performs a measurement on each member of a collection of quantum systems, prepared in the same unknown state. Each system is measured in a basis chosen from a complete set of measurements. The goal is to estimate the unknown state from the measurements results. This estimation can be done by different methods, but we study Maximum Likelihood Estimation (MLE), which finds among all possible states the one that maximizes the likelihood function. The likelihood function computes for any state the probability, according to that state, of obtaining the observed data.

Quantum homodyne tomography is one of the most popular optical tomography techniques available [44]. It rapidly became a versatile tool and has been applied in many different quantum optics experimental settings since it was proposed by Vogel and Risken in 1989 [5] and first implemented by Smithey *et al.* in 1993 [6]. This technique permits one to characterize an optical quantum state by analyzing multiple phase-sensitive measurements of the field quadratures.

A homodyne measurement generates a continuous value. It is a popular practice to discretize the measurement result, because this can considerably reduce the size of the data and expedite the reconstruction calculation. However, the discretization necessarily loses information contained in the original measurements. How should we choose a discretization strategy such that the bins are not too small nor too large? Larger bins will reduce calculation time and memory, but smaller bins will provide a better representation of the underlying distribution.

In this paper, we use numerical experiments to simulate optical homodyne tomography and perform maximum likelihood tomography on the data with and without discretization. When choosing a quadrature bin width, we use and compare two different strategies: Scott's rule [45] and Leonhardt's formula [46]. The paper is divided as follows: we begin by reviewing maximum likelihood in homodyne tomography in Sec. II. Then, in Sec. III, we describe our numerical experiments. Next, we discuss the estimation of the mean photon number from the quadrature measurements in Sec. IV. In Sec. V we present our results, and we make our concluding remarks in Sec. VI.

II. MAXIMUM LIKELIHOOD IN HOMODYNE TOMOGRAPHY

Let us consider N quantum systems, each prepared in an optical state described by a density matrix ρ_{true}. In each experimental trial i, we measure the field quadrature of one of the systems at some phase θ_i of a local oscillator, i.e., a reference system prepared in a high-amplitude coherent state. Each measurement is associated with an observable $\hat{X}_{\theta_i} = \hat{X}\cos\theta_i + \hat{P}\sin\theta_i$, where $\hat{X}$ and $\hat{P}$ are analogous to mechanical position and momentum operators, respectively. For a given phase θ_i, we measure a quadrature value x_i, resulting in the data $\{(\theta_i, x_i)|i = 1, \dots, N\}$.

*hilma@ufc.br

The outcome of the ith measurement is associated with a positive-operator-valued measure (POVM) element $\Pi(x_i|\theta_i) = \Pi_i$. Given the data, the likelihood of a candidate density matrix ρ is

$$\mathcal{L}(\rho) = \prod_{i=1}^{N} \mathrm{Tr}(\Pi_i \rho), \tag{1}$$

where $\mathrm{Tr}(\rho \Pi_i)$ is the probability density, when measuring with phase θ_i, to obtain outcome x_i, according to the candidate density matrix ρ.

MLE searches for the density matrix that maximizes the likelihood in Eq. (1). It usually is more convenient to maximize the logarithm of the likelihood (the "log-likelihood"):

$$L(\rho) = \ln \mathcal{L}(\rho) = \sum_{i=1}^{N} \ln[\mathrm{Tr}(\Pi_i \rho)], \tag{2}$$

which is maximized by the same density matrix as the likelihood. The MLE is essentially a function optimization problem, and since the log-likelihood function is concave, approximate convergence to a unique solution will be achieved by most iterative optimization methods.

In our numerical simulations, we use an algorithm for likelihood maximization that begins with iterations of the $R\rho R$ algorithm [47] followed by iterations of a regularized gradient ascent (RGA) algorithm. We switch from one algorithm to another because a slowdown is observed in the $R\rho R$ algorithm after about $(t+1)^2/4$ iterations, where $t + 1$ is the Hilbert space dimension. In the RGA, $\rho^{(k+1)}$ is parametrized as

$$\rho^{(k+1)} = \frac{(\sqrt{\rho^{(k)}} + A)(\sqrt{\rho^{(k)}} + A^\dagger)}{\mathrm{Tr}[(\sqrt{\rho^{(k)}} + A)(\sqrt{\rho^{(k)}} + A^\dagger)]}, \tag{3}$$

where $\rho^{(k)}$ is the density matrix found by the previous iteration, and A may be any complex matrix of the same dimensions as ρ. Equation (3) ensures that $\rho^{(k+1)}$ is a density matrix for any A. We then use sequential quadratic programming optimization strategy [48] in which A is chosen to maximize the quadratic approximation of the log-likelihood subject to $\mathrm{Tr}(AA^\dagger) \leqslant u$, where u is a positive number adjusted by the algorithm to guarantee that the log-likelihood increases with each iteration. To halt the iterations, we use the stopping criterion of Ref. [49], $L(\rho_{\mathrm{ML}}) - L(\rho^{(k)}) \leqslant 0.2$, where $L(\rho_{\mathrm{ML}})$ is the maximum of the log-likelihood, which ensures convergence to a state whose log-likelihood is very close to the maximum likelihood.

III. METHODS FOR NUMERICAL EXPERIMENTS

Our numerical experiments simulate single-mode optical homodyne measurements of three types of states: (1) superpositions of coherent states of opposite phase $|-\alpha\rangle + |\alpha\rangle$ (called "cat states"), (2) squeezed vacuum states, and (3) Fock states. Each state is represented by a density matrix ρ_{true} represented in the photon number basis, truncated at t photons. To better simulate realistic experiments, these pure states are subject to a 0.05 photon loss by passing through a medium with transmissivity of 0.95 before measurement.

In order to calculate the probability to obtain homodyne measurement outcome x, when measuring state ρ_{true} with phase θ, we represent all states and measurements in the photon number basis of a Hilbert space truncated at t photons. If $|x\rangle$ is the x-quadrature eigenstate with eigenvalue x, and $U(\theta)$ is the phase evolution unitary operator, then for an ideal homodyne measurement, we have $\Pi(x|\theta) = U(\theta)^\dagger |x\rangle\langle x| U(\theta)$. To include photon detector inefficiency, we replace the projector with $\Pi(x|\theta) = \sum_{i=1}^{n} E_i(\eta)^\dagger U(\theta)^\dagger |x\rangle\langle x| U(\theta) E_i(\eta)$, where η is the detection efficiency and $E_i(\eta)$ are the associated Kraus operators [44]. Typical state-of-the-art homodyne detection systems have efficiency $\eta \sim 0.9$, so we use this value in our simulations. Using this strategy, we are able to correct for the detector inefficiency as we estimate the state. We use rejection sampling from the distribution given by $P(x|\theta)$ to produce random samples of homodyne measurement results [50].

To choose the phases at which the homodyne measurements are performed, we divide the upper half-circle evenly among m phases between 0 and π and measure N/m times at each phase, where N is the total number of measurements. In all simulations, we use $m = 20$ and $N = 20\,000$. To secure a single maximum of the likelihood function, we need an informationally complete set of measurement operators, which can be obtained if we use $t + 1$ different phases to reconstruct a state that contains at most t photons [51].

To quantify the similarity of the reconstructed state ρ to the true state ρ_{true} we use the fidelity

$$F = \mathrm{Tr}\sqrt{\rho^{1/2} \rho_{\mathrm{true}} \rho^{1/2}}. \tag{4}$$

We report fidelities for four different situations: (i) the state is reconstructed using the continuous values of homodyne measurement results, that is, without discretization, (ii) the state is reconstructed with chosen bin widths, (iii) the state is reconstructed with bin widths given by Scott's rule [45], and (iv) the state is reconstructed with bin widths suggested by Leonhardt [51]. We consider only histograms with contiguous bins of equal width.

In 1979 Scott derived a formula recommending a bin width for discretizing data sampled from a probability density function f for a single random variable x. The recommended bin width is

$$h^\star = \left[\frac{6}{s \int_{-\infty}^{\infty} f'(x)^2 \, dx} \right]^{1/3}, \tag{5}$$

where the first and second derivatives of f must be continuous and bounded and s is the sample size. Because one does not know f in an experiment we assume a normal distribution. For a normal f we have

$$\int_{-\infty}^{\infty} f'(x)^2 \, dx = \frac{1}{4\sqrt{\pi}\sigma^3}, \tag{6}$$

where σ is the distribution's standard deviation. Combining Eqs. (5) and (6), we obtain the recommended bin width for a normal distribution:

$$h = 3.5 \, \sigma \, s^{-1/3}. \tag{7}$$

This formula is known as Scott's rule and is optimal for estimating f (minimizing total mean-squared error) at each phase if the data are normally distributed. In our simulations we compute a bin size separately for each phase's quadrature measurements, and we use the unbiased sample standard deviation in place of σ.

Although Scott's rule is optimal for each phase, it may not be optimal for homodyne tomography because we are estimating the density matrix rather than each phase's quadrature distribution individually. Also many interesting optical states do not have normal quadrature distributions, for example, our cat states. In fact, one might expect that the bin width should be related to the number of photons in a quantum state because higher photon number states have more narrow features in their quadrature distributions, which should not be washed out by the discretization.

Leonhardt states that if we desire to reconstruct a density matrix of a state with n photons, we need a bin width narrower than $q_n/2$, where q_n is given by

$$q_n = \frac{\pi}{\sqrt{2n+1}}. \tag{8}$$

This result was obtained from a semiclassical approximation for the amplitude pattern functions in quantum state sampling [46]. Leonhardt recommends using the maximum photon number in Eq. (8); however, many states have no maximum photon number, and whether a state has a maximum photon number is not possible to learn with certainty from tomography. Instead, we have tested using the photon number t at which the reconstruction Hilbert space is truncated and an estimate of the mean photon number $\overline{\langle \hat{n} \rangle}$ in Eq. (8). The truncation t must be chosen in advance to be large enough that the probability that ρ_{true} contains more than t photons is very small. We estimate the mean photon number from the quadrature measurements as described in the next section.

IV. ESTIMATING MEAN PHOTON NUMBER

In order to use Leonhardt's advice for choosing the histogram bin width, we need to estimate the mean number $\langle \hat{n} \rangle$ of photons in the measured state from the phase-quadrature data set. We use the estimator given in Refs. [52,53]. To obtain this estimator, we first compute the mean value of $(\hat{X}_\theta)^2$, averaged over θ, treating θ as if it is random and uniformly distributed between 0 and π:

$$\langle (\hat{X}_\theta)^2 \rangle = \langle \hat{X}^2 \cos^2\theta + (\hat{X}\hat{P} + \hat{P}\hat{X})\cos\theta\sin\theta + \hat{P}^2\sin^2\theta \rangle. \tag{9}$$

The phase θ is independent of $\hat{X}$ and $\hat{P}$, so we can compute the expectation over θ as

$$\langle (\hat{X}_\theta)^2 \rangle = \left\langle \int_0^\pi [\hat{X}^2\cos^2\theta + (\hat{X}\hat{P} + \hat{P}\hat{X})\cos\theta\sin\theta + \hat{P}^2\sin^2\theta]\text{Prob}(\theta)\,d\theta \right\rangle, \tag{10}$$

$$\langle (\hat{X}_\theta)^2 \rangle = \left\langle \int_0^\pi [\hat{X}^2\cos^2\theta + (\hat{X}\hat{P} + \hat{P}\hat{X})\cos\theta\sin\theta + \hat{P}^2\sin^2\theta]\frac{1}{\pi}\,d\theta \right\rangle \tag{11}$$

$$= \frac{1}{2}\langle \hat{X}^2 + \hat{P}^2 \rangle. \tag{12}$$

Because the photon number operator is

$$\hat{n} = \tfrac{1}{2}(\hat{X}^2 + \hat{P}^2 - 1), \tag{13}$$

we obtain

$$\langle \hat{n} \rangle = \langle \hat{X}_\theta^2 \rangle - \tfrac{1}{2}. \tag{14}$$

We estimate $\langle \hat{n} \rangle$ by computing the sample mean of all quadrature measurements [52,53]:

$$\overline{\langle \hat{n} \rangle} = \frac{1}{N}\sum_{i=1}^N x_i^2 - \frac{1}{2}, \tag{15}$$

where the bar above $\overline{\langle \hat{n} \rangle}$ distinguishes the true mean photon number from our estimate of the mean photon number. Note that when θ is uniformly distributed over $[0, \pi)$, the individual values of θ are not needed to compute $\overline{\langle \hat{n} \rangle}$.

V. RESULTS

To study the performance of various discretization strategies, we compute fidelities between the true state and the states estimated with the different strategies. Below ρ_{ML2} represents the state estimated without discretization, ρ_{Hist} is estimated with histogram bins of specified width chosen arbitrarily, ρ_{Scott} is estimated with bin widths chosen according to Scott's rule, and $\rho_{\text{Leonhardt}}$ is estimated with Leonhardt's bin widths. To make the graphs below, for each choice of parameters, we simulate 100 tomography experiments, making 100 density matrix estimates. The graphs show the arithmetic mean of the 100 fidelities of the reconstructed states. The half width of the error bars are the sample standard deviations of the 100 fidelities.

Our first results are shown in Fig. 1. The state considered is a cat state with $\alpha = 1$, where α is the amplitude of the coherent state in the superposition. The state is reconstructed in a Hilbert space truncated at $t = 10$ photons. (The probability that the $\alpha = 1$ state has more than 10 photons is 3.8×10^{-10}.) Scott's method finds a different optimal bin width for each phase considered, so we report the mean bin width averaged over the 20 phases in these cases. Here the mean bin width for Scott's method is 0.35. When choosing a bin width, we use values up to 0.34, the width we obtain when we use Eq. (8) for $t = 10$, the number of photons at which we truncated the Hilbert space. In all cases, each bin's measurement operator represents the measurement as if it occurred at the center of
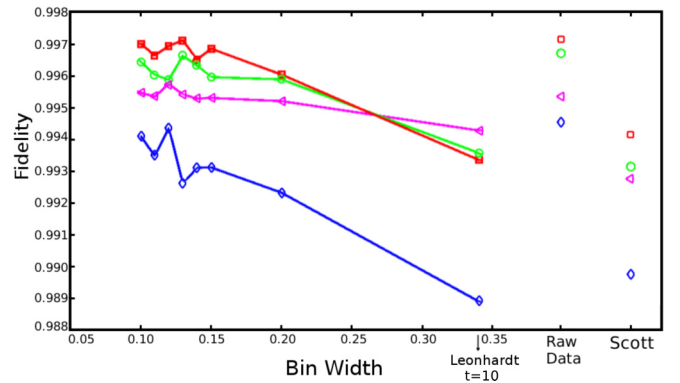

FIG. 1. Fidelities between estimated states and true states as functions of the bin width for a cat state with amplitude $\alpha = 1$ and photon loss of 0.05. The Hilbert space is truncated at $t = 10$ photons. Each set of points with the same color and marker shape corresponds to a different data set. The mean bin width for Scott method is 0.35.
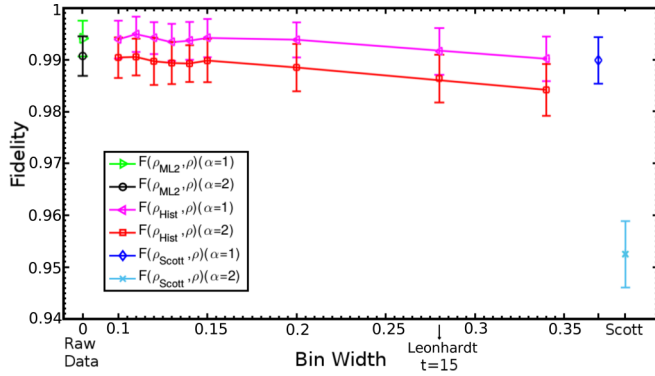
FIG. 2. Average fidelity as a function of the bin width for cat states with amplitudes $\alpha = 1$ and $\alpha = 2$. The Hilbert space is truncated at $t = 15$ photons. The mean bin widths for Scott's method are 0.35 ($\alpha = 1$ cat state) and 0.64 ($\alpha = 2$ cat state).

each bin. In Fig. 1 each set of points corresponds to a different data set. We see that different data sets had similar behavior as we changed the bin size. As we can see in this figure, the highest fidelities occur when we do not use discretization, as expected. We also see that smaller bin widths result in higher fidelities. However, even the largest bin widths tested result in a fidelity loss of only 0.005 compared to the raw data.

The next set of results is presented in Fig. 2, where we show average fidelities as a function of the bin width for cat states with amplitudes $\alpha = 1$ and $\alpha = 2$. The states are reconstructed in a $t = 15$ photons Hilbert space. The $\alpha = 2$ state has probability of 3.3×10^{-7} to contain more than 15 photons. The fidelity for an $\alpha = 1$ cat state is always greater than the fidelity for a $\alpha = 2$ cat state, including the case when we do not use discretization. This is expected, because a $\alpha = 2$ state requires more parameters to effectively describe its density matrix in the photon number basis, so for a given amount of data, there is greater statistical uncertainty.

For a given bin width the fidelity of the $\alpha = 2$ cat state estimates is always lower than the fidelity for the $\alpha = 1$ cat state estimates. This is also expected because the $\alpha = 2$ state has more wiggles in its probability distribution, so more information is lost when the bins are larger. The average bin width used by Scott's method is 0.35 for the $\alpha = 1$ cat state, and 0.64 for the $\alpha = 2$ cat state, which results in significant
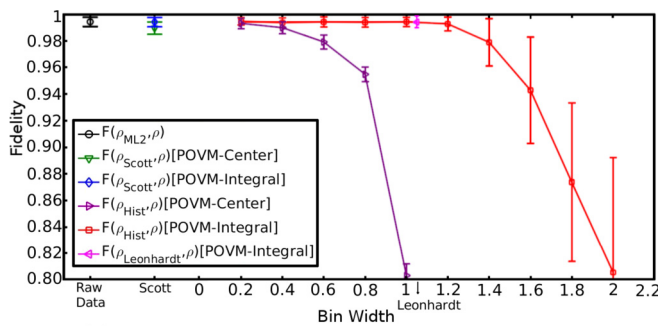
fidelity loss. Leonhardt's width indicated in Fig. 2 is obtained by using $t = 15$ in place of n in Eq. (8).

Until now, as mentioned before, every measurement outcome in a given bin has been associated with the measurement operator for the quadrature value at the center of that bin. That is, the measurement operator Π_i associated with bin i would give the probability density of obtaining a measurement result at the center of bin i when computing $\text{Tr}(\Pi_i \rho)$. Although this may be a useful approximation for very small bins, to improve our analysis, we now change each bin's measurement operator so that it represents a measurement that occurs anywhere in the bin. To obtain these new operators, we numerically integrate the measurement operators over the width of each histogram bin. With these integrated measurement operators, computing $\text{Tr}(\Pi_i \rho)$ will gives the probability to obtain a measurement result anywhere in bin i. We identify each case by adding [POVM-center] and [POVM-integral] to the legends in the graphs.

We also add to our analysis the use of the mean photon number estimate in Leonhardt's formula, and we calculate the fidelity between ρ_{true} and the state $\rho_{\text{Leonhardt}}$ estimated using the resulting bin width. Recall that Leonhardt recommends
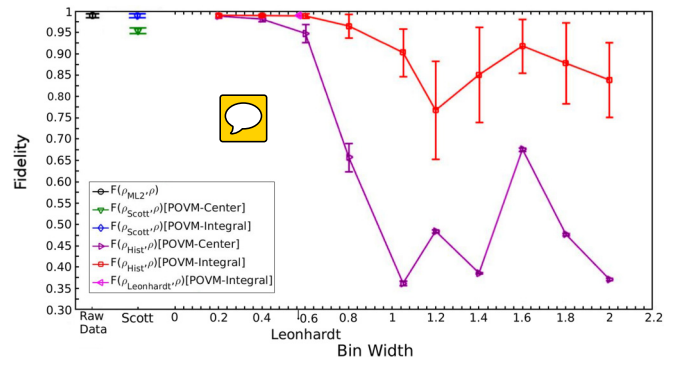

FIG. 4. Average fidelity as a function of the bin width for a cat state with amplitude $\alpha = 2$. The Hilbert space is truncated at $t = 15$ photons. For this state, $\langle n \rangle = 3.1978$, and $\overline{\langle \hat{n} \rangle} = 3.1983$, giving a bin width by Leonhardt's formula of 0.58. The mean bin width for Scott's method is 0.64.

FIG. 3. Average fidelity as a function of the bin width for a cat state with amplitude $\alpha = 1$. The Hilbert space is truncated at $t = 10$ photons. For this state, $\langle n \rangle = 0.6093$, and $\overline{\langle \hat{n} \rangle} = 0.6109$, giving a bin width by Leonhardt's formula of 1.05. The mean bin width for Scott's method is 0.35.
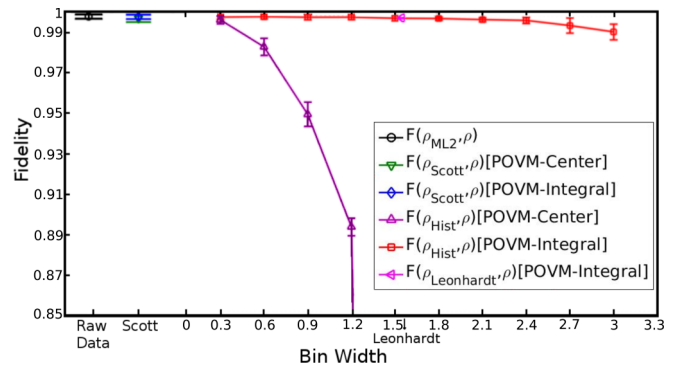

FIG. 5. Average fidelity as a function of the bin width for a squeezed vacuum state whose squeezed quadrature has a variance $3/4$ of the vacuum variance. The Hilbert space is truncated at $t = 10$ photons. For this state, $\langle n \rangle = 0.0167$, and $\overline{\langle \hat{n} \rangle} = 0.0162$, giving a bin width by Leonhardt's formula of 1.54. The mean bin width for Scott's method is 0.25.
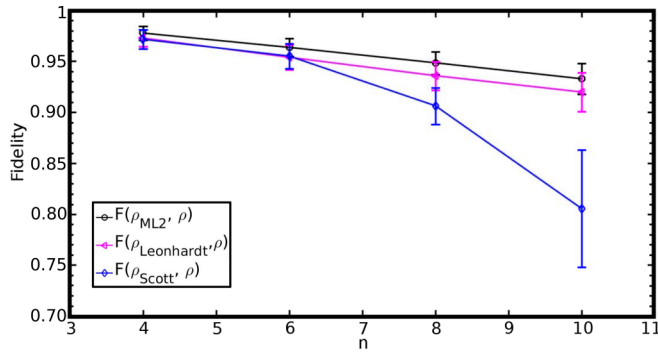
FIG. 6. Average fidelities as functions of bin width for Fock states with different numbers of photons n. The bin widths from Leonhardt's formula are 0.56 ($n = 4$), 0.46 ($n = 6$), 0.40 ($n = 8$), and 0.36 ($n = 10$). The mean bin width from Scott's method are 0.69 ($n = 4$), 0.82 ($n = 6$), 0.95 ($n = 8$), and 1.05 ($n = 10$).

that the bin width should be smaller than the one calculated using the maximum photon number in Eq. (8), but here we use the estimate of the mean photon number instead.

Figures 3 and 4 show average fidelities as functions of the bin width for cat states with amplitudes $\alpha = 1$ and $\alpha = 2$, respectively. Figure 5 examines a squeezed vacuum state whose squeezed quadrature has a variance 3/4 of the vacuum variance. Note for the cat states, as α increases, Scott's bin width also increases, which is certainly undesirable because the quadrature distributions contain more fine structure. These graphs show that integrating the measurement operators over the width of each bin considerably improves the fidelities for all cases. We can also see that Leonhardt's suggestion using the estimated mean photon number can be safely used as the upper bound for the bin width.

As seen in Eq. (7), Scott's rule gives bin widths proportional to the sample standard deviation. Since states with a higher number of photons can have higher standard deviations, Scott's method will produce larger bin widths. This is undesirable because pure states containing many photons have very fine features in their quadrature distributions. On the other hand, we expect Leonhardt's method to perform better because it uses the estimated mean number of photons to calculate the
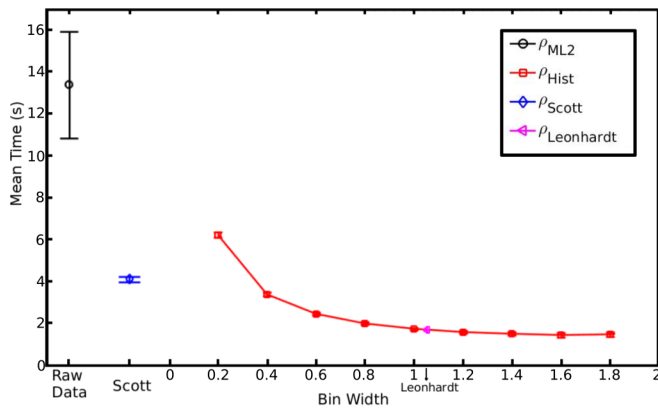

FIG. 7. Average reconstruction time as a function of the bin width for a cat state with amplitude $\alpha = 1$. The Hilbert space is truncated at $t = 10$ photons. The mean bin width for Scott's method is 0.35, and the bin width given by Leonhardt's formula is 1.05.
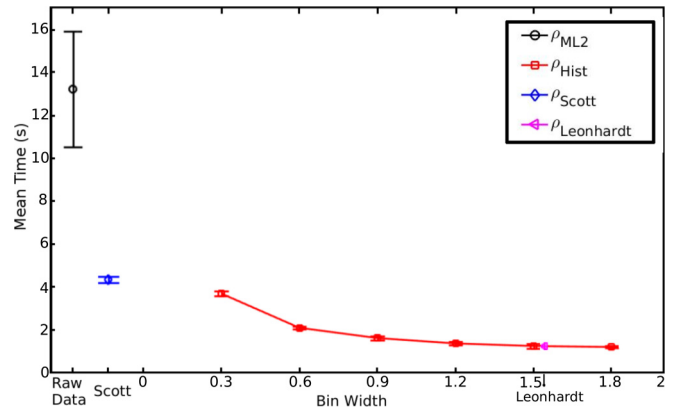

FIG. 8. Average reconstruction time as a function of the bin width for a squeezed vacuum state whose squeezed quadrature has a variance 3/4 of the vacuum variance. The Hilbert space is truncated at $t = 10$ photons. The mean bin width for Scott's method is 0.25, and the bin width given by Leonhardt's formula is 1.54.

bin width. We can clearly see the expected behavior of both methods for higher numbers of photons in Fig. 6, where we have used Fock states to check our claim.

All of the discretization methods considered here give much faster fidelity estimates, as we can see in Figs. 7 and 8, with no significant loss of fidelity between the estimated states and the true states. The average times reported here include any calculations required to determine the desired bin width from the original homodyne data, the construction of histograms, and the ML density matrix estimation. All the simulations were carried out in a dual-core computer running at 3.7 GHz with 4 GB of RAM.

VI. CONCLUSION

We have used idealized numerical experiments to generate simulated data, performed maximum likelihood tomography on data sampled from cat states and squeezed vacuum states with and without discretization, and estimated the fidelities between the reconstructed states and the true state. We used two different methods to choose the bin width: Scott's and Leonhardt's methods. We studied using measurement operators calculated using the quadrature exactly at the center of each bin and integrating the measurement operators along the length of the bin.

Scott's method calculates an optimal bin width, for each phase, based on the size and the standard deviation of the sample. This method works well for Gaussian states and states with small numbers of photons. States with higher number of photons have quadrature distributions with higher standard deviations, giving bigger bin widths for each phase. We implemented Scott's method for Gaussian distributions, but if one has prior knowledge about the state and its distribution, one could tailor Scott's rule by using more appropriate distributions in Eq. (5).

Leonhardt's method recommends a bin width narrower than $q_n/2$, where q_n decreases with the square root of the number of photons in the state being reconstructed. Since, in a real experiment, we do not know the mean number of photons in the state considered, we estimate the mean photon number from the quadrature measurement results. We have found

360 that the method to find the mean number of photons from
361 the quadrature measurement results gives accurate results.
362 We checked that by comparing the estimated mean number
363 of photons with the true mean number of photons for the
364 cat states and squeezed vacuum states. We also have found
365 that integrating the measurement operators over the width of
366 each histogram bin significantly improves the fidelity. Using
367 this strategy, Leonhardt's formula safely establishes an upper
368 bound to the bin width, and both methods provides a faster
369 statistical estimation without losing too much information.

[1] A. Kandala, A. Mezzacapo, K. Temme, M. Takita, M. Brink, J. M. Chow, and J. M. Gambetta, Hardware-efficient quantum optimizer for small molecules and quantum magnets, Nature (London) **549**, 242 (2014).

[2] N. M. Linke, D. Maslov, M. Roetteler, S. Debnath, C. Figgatt, K. A. Landsman, K. Wright, and C. Monroe, Experimental comparison of two quantum computing architectures, Proc. Natl. Acad. Sci. USA **114**, 3305 (2017).

[3] T. Monz, D. Nigg, E. A. Martinez, M. F. Brandl, P. Schindler, R. Rines, S. X. Wang, I. L. Chuang, and R. Blatt, Realization of a scalable Shor algorithm, Science **351**, 1068 (2017).

[4] V. S. Denchev, S. Boixo, S. V. Isakov, N. Ding, R. Babbush, V. Smelyanskiy, J. Martinis, and H. Neven, What is the Computational Value of Finite-Range Tunneling?, Phys. Rev. X **6**, 031015 (2016).

[5] K. Vogel and H. Risken, Determination of quasiprobability distributions in terms of probability distributions for the rotated quadrature phase, Phys. Rev. A **40**, 2847 (1989).

[6] D. T. Smithey, M. Beck, M. G. Raymer, and A. Faridani, Measurement of the Wigner Distribution and the Density Matrix of a Light Mode Using Optical Homodyne Tomography: Application to Squeezed States and the Vacuum, Phys. Rev. Lett. **70**, 1244 (1993).

[7] T. J. Dunn, I. A. Walmsley, and S. Mukamel, Experimental Determination of the Quantum-Mechanical State of a Molecular Vibrational Mode Using Fluorescence Tomography, Phys. Rev. Lett. **74**, 884 (1995).

[8] K. Banaszek, C. Radzewicz, K. Wodkiewicz, and J. S. Krasinski, Direct measurement of the Wigner function by photon counting, Phys. Rev. A **60**, 674 (1999).

[9] K. Banaszek, G. M. D'Ariano, M. G. A. Paris, and M. F. Sacchi, Maximum-likelihood estimation of the density matrix, Phys. Rev. A **61**, 010304(R) (1999).

[10] A. G. White, D. F. V. James, W. J. Munro, and P. G. Kwiat, Exploring Hilbert space: Accurate characterization of quantum information, Phys. Rev. A **65**, 012301 (2001).

[11] A. Ourjoumtsev, H. Jeong, R. Tualle-Brouri, and P. Grangier, Generation of optical 'Schrödinger cats' from photon number states, Nature (London) **448**, 784 (2007).

[12] J. S. Neergaard-Nielsen, B. M. Nielsen, C. Hettich, K. Mølmer, and E. S. Polzik, Generation of a Superposition of Odd Photon Number States for Quantum Information Networks, Phys. Rev. Lett. **97**, 083604 (2006).

[13] I. L. Chuang and M. A. Nielsen, Prescription for experimental determination of the dynamics of a quantum black box, J. Mod. Optics **44**, 2455 (1997).

[14] J. F. Poyatos, J. I. Cirac, and P. Zoller, Complete Characterization of a Quantum Process: The Two-Bit Quantum Gate, Phys. Rev. Lett. **78**, 390 (1997).

[15] J. B. Altepeter, D. Branning, E. Jeffrey, T. C. Wei, P. G. Kwiat, R. T. Thew, J. L. O'Brien, M. A. Nielsen, and A. G. White, Ancilla-Assisted Quantum Process Tomography, Phys. Rev. Lett. **90**, 193601 (2003).

[16] G. M. D'Ariano and L. Maccone, Measuring Quantum Optical Hamiltonians, Phys. Rev. Lett. **80**, 5465 (1998).

[17] M. A. Nielsen, E. Knill, and R. Laflamme, Complete quantum teleportation using nuclear magnetic resonance, Nature (London) **396**, 52 (1998).

[18] M. W. Mitchell, C. W. Ellenor, S. Schneider, and A. M. Steinberg, Diagnosis, Prescription and Prognosis of a Bell-State Filter by Quantum Process Tomography, Phys. Rev. Lett. **91**, 120402 (2003).

[19] J. L. O'Brien, G. J. Pryde, A. Gilchrist, D. F. V. James, N. K. Langford, T. C. Ralph, and A. G. White, Quantum Process Tomography of a Controlled-Not Gate, Phys. Rev. Lett. **93**, 080502 (2004).

[20] C. Kupchak, S. Rind, B. Jordaan, and E. Figueroa, Quantum Process Tomography of an Optically-Controlled Kerr Non-Linearity, Sci. Rep. **5**, 16581 (2015).

[21] A. Luis and L. L. Sanchez-Soto, Complete Characterization of Arbitrary Quantum Measurement Processes, Phys. Rev. Lett. **83**, 3573 (1999).

[22] J. Fiurasek, Maximum-likelihood estimation of quantum measurement, Phys. Rev. A **64**, 024102 (2001).

[23] G. M. D'Ariano, L. Maccone, and P. Lo Presti, Quantum Calibration of Measurement Instrumentation, Phys. Rev. Lett. **93**, 250407 (2004).

[24] J. S. Lundeen, A. Feito, H. Coldenstrodt-Ronge, K. L. Pregnell, Ch. Silberhorn, T. C. Ralph, J. Eisert, M. B. Plenio, and I. A. Walmsley, Tomography of quantum detectors, Sci. Rep. **5**, 27 (2009). **Q**

[25] S. Lloyd and S. L. Braunstein, Quantum Computation Over Continuous Variables, Phys. Rev. Lett. **82**, 1784 (1999).

[26] D. Gottesman, A. Kitaev, and J. Preskill, Encoding a qubit in an oscillator, Phys. Rev. A **64**, 012310 (2001).

[27] S. D. Bartlett, H. de Guise, and B. C. Sanders, Quantum encodings in spin systems and harmonic oscillators, Phys. Rev. A **65**, 052316 (2002).

[28] H. Jeong and M. S. Kim, Efficient quantum computation using coherent states, Phys. Rev. A **65**, 042305 (2002).

[29] T. C. Ralph, A. Gilchrist, G. J. Milburn, W. J. Munro, and S. Glancy, Quantum computation with optical coherent state, Phys. Rev. A **68**, 042319 (2003).

[30] T. Ralph, Continuous variable quantum cryptography, Phys. Rev. A **61**, 010303(R) (1999).

[31] M. Hillery, Quantum cryptography with squeezed states, Phys. Rev. A **61**, 022309 (2000).

[32] Ch. Silberhorn, T. C. Ralph, N. Lütkenhaus, and G. Leuchs, Continuous Variable Quantum Cryptography: Beating the 3 db Loss Limit, Phys. Rev. Lett. **89**, 167901 (2002).

[33] S. Pirandola, S. Mancini, S. Lloyd, and S. L. Braunstein, Continuous-variable quantum cryptography using two-way quantum communication, Nat. Phys. **4**, 726 (2008).

[34] F. S. Luiz and G. Rigolin, Teleportation-based continuous variable quantum cryptography, Quantum Inf. Proc. **16**, 58 (2017).

[35] T. Eberle, S. Steinlechner, J. Bauchrowitz, V. Händchen, H. Vahlbruch, M. Mehmet, H. Müller-Ebhardt, and R. Schnabel, Quantum Enhancement of the Zero-Area Sagnac Interferometer Topology for Gravitational Wave Detection, Phys. Rev. Lett. **104**, 251102 (2010).

[36] R. Demkowicz-Dobrzanski, K. Banaszek, and R. Schnabel, Fundamental quantum interferometry bound for the squeezed-light-enhanced gravitational wave detector GEO 600, Phys. Rev. A **88**, 041802(R) (2013).

[37] L. Vaidman, Teleportation of quantum states, Phys. Rev. A **49**, 1473 (1994).

[38] S. L. Braunstein and H. J. Kimble, Teleportation of Continuous Quantum Variables, Phys. Rev. Lett. **80**, 869 (1998).

[39] Q. He, L. Rosales-Zárate, G. Adesso, and M. D. Reid, Secure Continuous Variable Teleportation and Einstein-Podolsky-Rosen Steering, Phys. Rev. Lett. **115**, 180502 (2015).

[40] S. L. Braunstein and H. J. Kimble, Dense coding for continuous variables, Phys. Rev. A **61**, 042302 (2000).

[41] J. Lee, S. W. Ji, J. Park, and H. Nha, Continuous-variable dense coding via a general Gaussian state: Monogamy relation, Phys. Rev. A **90**, 022301 (2014).

[42] N. J. Cerf and S. Iblisdir, Optimal *N*-to-*M* cloning of conjugate quantum variables, Phys. Rev. A **62**, 040301(R) (2000).

[43] S. L. Braunstein, N. J. Cerf, S. Iblisdir, P. van Loock, and S. Massar, Optimal Cloning of Coherent States with a Linear Amplifier and Beam Splitters, Phys. Rev. Lett. **86**, 4938 (2001).

[44] A. I. Lvovsky, Iterative maximum-likelihood reconstruction in quantum homodyne tomography, J. Opt. B **6**, S556 (2004).

[45] D. Scott, Scott's rule, WIREs Comp. Stat. **2**, 497 (2010).

[46] U. Leonhardt, M. Munroe, T. Kiss, T. Richter, and M. G. Raymer, Sampling of photon statistics and density matrix using homodyne detection, Opt. Commun. **127**, 144 (1996).

[47] J. Řeháček, Z. Hradil, E. Knill, and A. I. Lvovsky, Diluted maximum-likelihood algorithm for quantum tomography, Phys. Rev. A **75**, 042108 (2007).

[48] J. Nocedal and S. J. Wright, *Numerical Optimization*, 2nd ed., Springer Series in Operations Research and Financial Engineering (Springer Science+Business Media, New York, 2006), Ch. 18.   **2**

[49] S. C. Glancy, E. Knill, and M. Girard, Gradient-based stopping rules for maximum-likelihood quantum-state tomography, New J. Phys. **14**, 095017 (2012).

[50] W. J. Kennedy Jr. and J. E. Gentle, *Statistical Computing* (Marcel Dekker, New York, 1980), section 6.4.3.   **3**

[51] U. Leonhardt, *Measuring the Quantum State of Light* (Cambridge University Press, New York, 1997).

[52] M. G. Raymer and M. Beck, Experimental quantum state tomography of optical fields and ultrafast statistical sampling, in *Quantum State Estimation*, Vol. 649, edited by M. G. A. Paris and J. Řehček (Springer, New York, 2004), p. 259.

[53] M. Munroe, Ultrafast photon statistics of cavityless laser light, Ph.D. thesis, University of Oregon (1996).